Microelectronic Engineering 153 (2016) 11–14

Contents lists available at ScienceDirect

Microelectronic Engineering

journal homepage: www.elsevier.com/locate/mee

Development of InSb dry etch for mid-IR applications

Vincenzo Pusino *, Chengzhi Xie, Ata Khalid, Iain G. Thayne, David R.S. Cumming

Electronics and Nanoscale Division, School of Engineering, University of Glasgow, Glasgow G12 8QQ, UK

ARTICLE INFO

Article history:
Received 20 October 2015
Received in revised form 18 December 2015
Accepted 21 December 2015
Available online 22 December 2015

Keywords:
Inductive coupled plasma
Etching
III–V semiconductors
InSb
GaSb
Microfabrication

ABSTRACT

We present a new chlorine-free dry etching process which was used to successfully etch indium antimonide grown on gallium arsenide substrates while keeping the substrate temperature below 150 °C. By use of a reflowed photoresist mask a sidewall with 60 degree positive slope was achieved, whereas a nearly vertical one was obtained when hard masks were used. Long etch tests demonstrated the non-selectivity of the process by etching through the entire multi-layer epitaxial structure. Electrical and optical measurements on devices fabricated both by wet and dry etch techniques provided similar results, proving that the dry etch process does not cause damage to the material. This technique has a great potential to replace the standard wet etching techniques used for fabrication of indium antimonide devices with a non-damaging low temperature plasma process.

1. Introduction

In the medium infrared (mid-IR) wavelength range, indium antimonide (InSb), has a high potential for sensing applications and InSb-based Focal Plane Arrays (FPAs) have been demonstrated [1] and commercialised. InSb patterning techniques typically utilise wet-chemical etching, with solutions based on citric acid ($C_6H_8O_7$), water (H_2O) and hydrogen peroxide (H_2O_2) being established wet etchants for antimonides [2]. However, the introduction of a consistent and reliable dry etch process could improve several drawbacks encountered with wet etching, such as uniformity and galvanic corrosion issues [3] and the fact that its isotropic nature also limits the minimum pixel size and the fill factor of fabricated detector arrays. Dry etching of InSb was reported in several publications [4–6], and in most cases was achieved through an inductively coupled plasma (ICP) process involving chlorine-containing compounds such as BCl_3 and Cl_2 [7,8]. However, their use for etching of InSb causes the formation of highly non-volatile indium chloride ($InCl_3$) by-products, which require temperatures in excess of 200 °C to be successfully purged. InSb epi-structures grown by Molecular Beam Epitaxy (MBE) on gallium arsenide (GaAs) substrates, which have been subject of increased research interest in recent years, cannot withstand such high temperatures, since antimony desorption phenomena are triggered and result in material degradation causing poor operation of the fabricated devices. In a similar way, the material can deteriorate if it is subject to strong radio frequency (RF) plasmas. These widely reported issues [9–11] make fabrication on MBE-grown InSb particularly challenging. Here we report on a new dry etch process which was successfully used on MBE-grown InSb without related damage. Furthermore, two different etch profiles were obtained depending on the type of mask used.

The structure of this work is the following: Section 2 describes the epi-structure of the material used and the development of technique presented. Section 3 discusses the main results, with the conclusions drawn from them presented in Section 4.

2. Material and methods

The material structure used in this work, shown in Fig. 1, was designed to achieve a monolithically integrated mid-IR pixel. It therefore consists of an InSb p–i–n structure for implementation of a mid-IR sensing photodiode (PD), and of an underlying MEtal Semiconductor Field Effect Transistor (MESFET) to be used for switching [12]. Since the PD and the MESFET are to be connected together but a significant non-planarity of the structure exists, a dry etch process able to provide positively sloped sidewalls was sought to facilitate metal interconnects. For the reasons explained in the Introduction, attention turned to chlorine free processes since they were more likely to work at room temperature. The most widely reported chlorine-free process suitable for dry etching of InSb was based on $CH_4/H_2/Ar$ [13,14] therefore the same gas mixture was chosen as starting point for process development.

The tool used was the Plasmalab 100 Inductively Coupled Plasma (ICP) 180 etching tool from Oxford instruments. All samples etched were mounted on a 6 inch silicon carrier wafer by means of thermal grease, to ensure a good thermal contact. Irreversible temperature indicators were placed on the carrier to monitor the maximum temperature reached in the chamber due to the etching plasma. Samples prepared for etching all underwent the same cleaning procedure consisting of

* Corresponding author.
E-mail address: Vincenzo.Pusino@glasgow.ac.uk (V. Pusino).

http://dx.doi.org/10.1016/j.mee.2015.12.014
0167-9317/

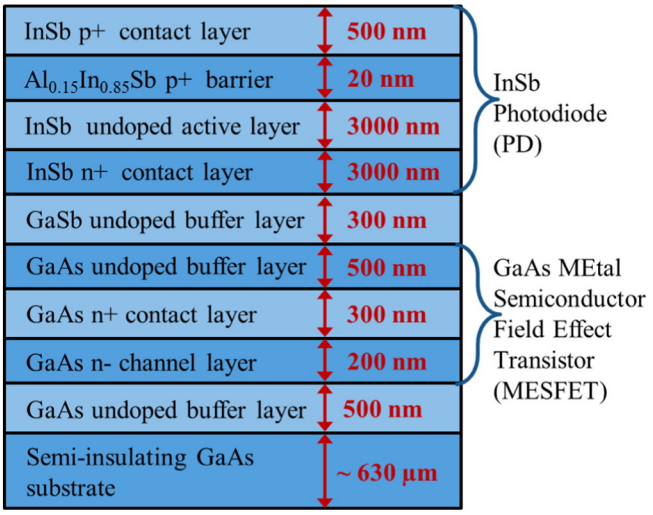

Fig. 1. Layer structure of the material used.

OptiClear™, acetone, isopropyl alcohol soak and de-ionised (DI) water rinse prior to the definition of the mask. Ultrasonic baths were not used during the cleaning procedure in order to avoid inducing damage to the material. Tests were carried out using three types of masks: Silicon nitride (SiN_x), deposited at room temperature in an ICP reactor; Hydrogen silsesquioxane (HSQ), a negative-tone resist patterned by electron beam lithography; and Shipley AZ4562 resist, a positive-tone photolithography resist. The outcome of each etch test was assessed in the first instance by a profilometer, then samples were cleaved and their cross-section examined by Scanning Electron Microscope (SEM). The etch tests carried out explored a range of chamber pressures, gas flows, ICP and RF power. The results from process optimisation for each of these masks are presented in the next section.

3. Results and discussion

For all of the investigated etch masks, the best results were obtained with an ICP power of 600 W, an RF power of 150 W, a chamber pressure of 15 mT, and a table temperature of 110 °C. These parameters provided a DC bias of −315 V. The next subsections will present the results of the various types of etching masks used.

3.1. AZ4562 photoresist mask

When an AZ4562 photoresist mask was used, the etch profile with a positive slope of approximately 60° shown by the SEM images in Fig. 2 was obtained, with a $CH_4/H_2/Ar$ flow of 15/50/5 sccm and a post-development hard bake of the AZ4562. Subjecting the resist mask to a hard bake between lithography and etching was found to be crucial to achieve a positively sloped etch profile; the subsequent resist reflow caused the mask to acquire a dome-shaped profile whose gradual erosion by the RF plasma translated into a sloped etch. This optimised recipe had an 80 nm/min average etch rate on InSb and a selectivity of 2:1. The maximum sidewall roughness was estimated from SEM images to be approximately 50 nm. This value is most likely due to a direct transfer of the edge roughness of the photoresist mask used, and could be improved by changes in the photoresist reflow process, such as the use of plasma assisted reflow [15] or by the addition of nitrogen to the etching RF plasma [16].

Long etches were also investigated, to assess the potential of the process to etch through the heterogeneous layers composing the material structure, and they proved the non-selectivity of the process for the etching of InSb, GaSb and GaAs, as Fig. 2c and d shows. The developed recipe also etched through the 20 nm $Al_{0.15}In_{0.85}Sb$ barrier layer whereas generally aluminium-containing III–V compounds act as etch stop layers for CH_4/H_2 chemistries [17]. The etching mechanism here is thought to be based on trimethylaluminium formation [18]. With regard to the etching of the InSb layers, despite previous work on different materials showing doping level-dependent etch characteristics [19] and plasma-induced doping type conversion [20], no change in etch rate or slope was observed between the p-doped, intrinsic, and n-doped InSb layers. Samples used for the long etch test were etched for 90 min without cooling nitrogen purges in between, and the temperature indicators showed a temperature rising to approximately 145 °C by the end of the run. Despite this temperature still well tolerated by our material, for etch rate consistency and etch controllability it is best if the temperature is kept constant through the etch process. This was found to be possible if 5 min nitrogen purges were introduced every 15 min of etching, in order to keep the chamber at the initial 110 °C. Since this temperature is close to the glass transition of AZ4562 [21], the dry etch process is equivalent to a long hard bake, and resist removal following the etch process was found to be problematic. Long soaks in warm (50 °C) acetone were found to be ineffective for mask removal, while SVC-14™ resist stripper provided better results, however leaving behind a significant amount of residues which required oxygen plasma to be cleared. Solvents containing n-methyl-2-pyrrolidone (NMP) such as MICROPOSIT 1165™ were not tested for AZ4562 removal since they were found to corrode the material epitaxial layers, something that was previously reported for other III–V materials [3]. A slight modification in the process which simplified stripping the resist post-etch was the use of a dual layer mask, consisting of LOR 10A underlying AZ4562. LOR series resists are based on polydimethylglutarimide and have a glass transition temperature of 180 °C [22], well in excess of that of AZ4562 and also above the maximum temperature reached during the dry etch process. Fig. 3 compares post-etch SEM images from two samples after an overnight soak in SVC-14™, with the stripped mask consisting either of AZ4562 only (Fig. 3a) or of a dual layer of AZ4562 and LOR resists (Fig. 3b): a reduction in resist residue is clearly visible.

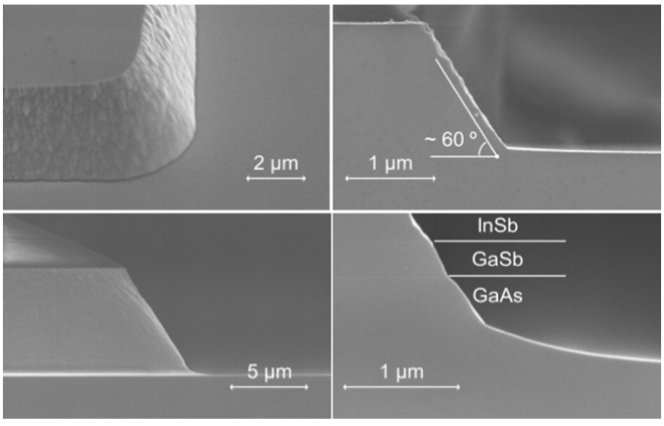

Fig. 2. SEM images showing the results of a 15 minute (a,b) and 90 minute (c,d) etching with AZ4562 mask and optimised $CH_4/H_2/Ar$ gas flow.

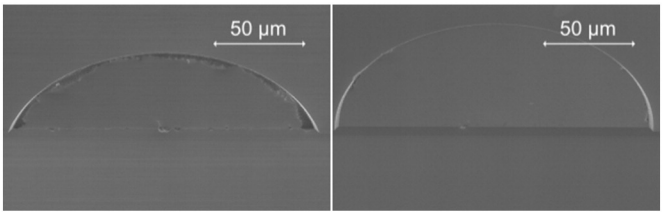

Fig. 3. SEM images comparing resist residues for a (a) AZ4562 only mask and (b) a dual layer of LOR 10A and AZ4562.

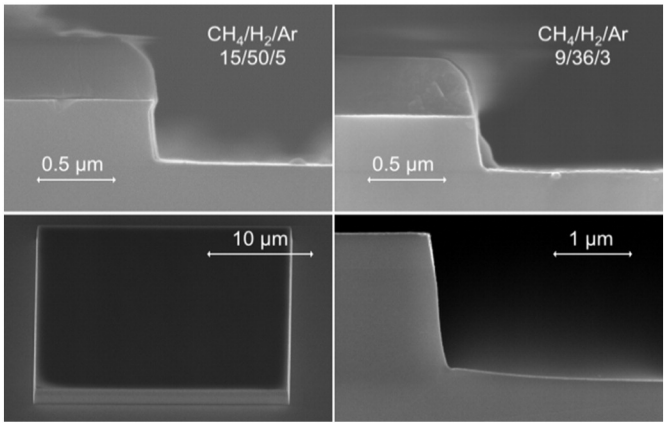

Fig. 4. SEM images of samples etched with a hard mask: non-optimised (a) or optimised gas flow ratio (b) for a SiN_x mask; etched mesa (c) and its cross-section (d) if an HSQ mask was used with the optimised gas flow ratio.

3.2. SiN_x and HSQ masks

When the process parameters described in Section 3.1 were used to etch samples with a SiN_x mask, an undercut profile was obtained, as shown in Fig. 4a. A nearly vertical profile (approximately 85 degrees) could instead be achieved with further dilution of the gases used, going from gas flow ratio of 15/50/5 sccm to 9/36/3 ratio, which gave the results shown in Fig. 4b. In both cases the etch rate was lower than with the AZ4562 mask, with 57 and 53 nm/min for the undercut and nearly vertical etch, respectively. Similar results were obtained by use of an HSQ mask, with the outcome shown in Fig. 4c and d. Again, the process employing more diluted gases provided an etch rate of 50 nm/min and a slope of approximately 85°. The smooth profile of the sidewall is a further confirmation that the etch roughness observed for the AZ4562 resist was due to the mask roughness. The use of hard masks was not investigated further since the purpose of this work was to achieve a positively sloped etch to facilitate metal interconnects.

3.3. Plasma damage assessment

Ion bombardment experienced by the material during plasma processing can cause damage to the exposed surfaces [11] and result in poorer operation of devices fabricated by dry etch when compared to those not subject to RF plasmas. In order to assess the effect of the developed etch process on our material structure, we fabricated two batches of InSb PDs, with the only difference between them being the mesa etching step. The reference wet etched devices underwent

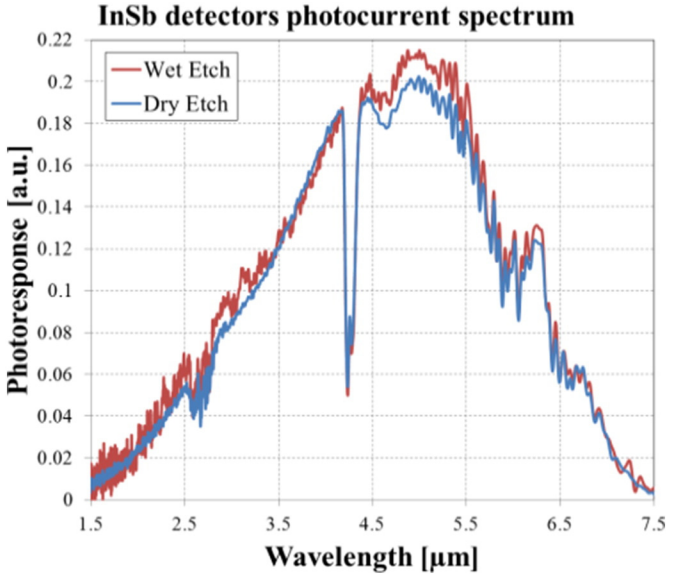

Fig. 6. Photocurrent spectrum comparison between wet and dry etched InSb PDs.

the following fabrication processes: mesas were defined using standard photolithography techniques (Shipley Microposit S1818 series Photoresist), then the pattern was transferred onto the material by a subsequent wet etch in a solution of citric acid and hydrogen peroxide, a widespread wet etchant for InSb [2], targeting an etch depth of 3.5 μm. The sizes of the fabricated mesa were squares with 800 μm side for ease of probing/bonding. Following wet etch and resist strip, Ohmic contacts were defined at the same time for the n-doped and p-doped layers using a bi-layer of photoresist to lift off a Ti–Au film deposited by metal evaporation. The annealing of the contacts was not necessary thanks to the narrow band-gap of InSb (0.17 eV at 300 K). The fabrication flow for the dry etch devices was identical to the reference ones except that AZ4562 was used as photolithographic mask and that the sample was etched in the ICP 180 tool for 45 min with the parameters mentioned in Section 3.1 to achieve a 3.5 μm etch depth.

I–V characterisation at room temperature and at 77 K was carried out for both samples, with the results shown in Fig. 5. At 300 K due to the narrow band-gap of InSb the I–V curve is dominated by thermally excited carriers and no rectification is present. A clear rectifying behaviour is instead observed at 77 K. It was observed that the dry etched devices provided better device uniformity with regards to the current measured under reverse bias. At room temperature an average dark current of −2 mA was measured under 5 mV reverse bias for both wet etch and dry etch cases, decreasing to approximately 100 μA (again for both cases) when the InSb PDs were cooled.

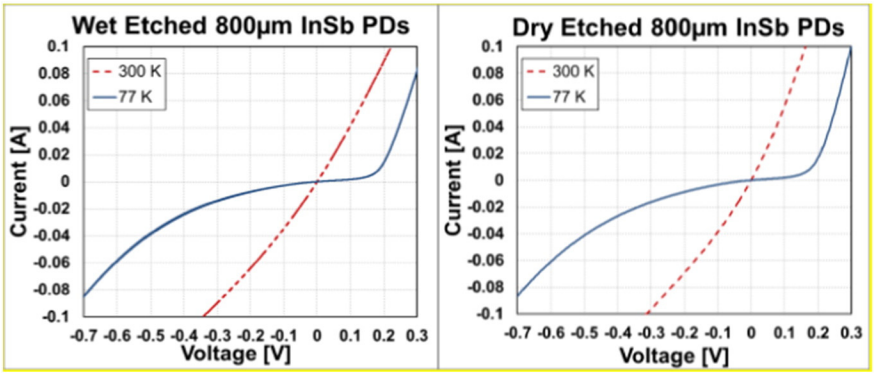

Fig. 5. Comparison between I–V characteristics of wet etched (a) and dry etched (b) 800 μm InSb PDs at room temperature (dashed red line) and cooled with liquid nitrogen (continuous blue line). (For interpretation of the references to colour in this figure legend, the reader is referred to the web version of this article.)

The wet etched and dry etched devices were also compared in terms of relative photoresponse at room temperature, measured by means of a Bruker Vertex 70 FTIR spectrometer. Fig. 6 compares the photocurrent spectra between wet etched and dry etched devices, and once again the results are comparable. The sudden drop in photoresponse at the wavelength of 4.2 μm is caused by carbon dioxide absorption since the measurements were carried out in standard atmosphere.

From the I–V and photoresponse assessment it can be concluded that the inclusion of the developed dry etch process as part of the fabrication flow does not impair the electrical operation of the InSb PDs, nor their ability to detect the mid-IR light.

4. Conclusions

We developed a low-temperature chlorine-free dry etch process suitable for etching of MBE-grown InSb layers. The process proved its non-selectivity by etching through the entire material stack, consisting of InSb, GaSb and GaAs layers. A positively sloped etched profile was obtained if reflowed AZ4562 photoresist was used as a mask, whereas the use of hard masks (HSQ, SiN_x) provided a nearly vertical etch. InSb PDs fabricated by standard wet etch techniques were compared to devices where the mesa was dry etched, and the developed process was found not to hinder the device conduction or its photoresponse. The developed process is thought to have the potential to replace the standard wet etch techniques used in antimonide fabrication.

Acknowledgements

The authors gratefully acknowledge the financial support provided by EPSRC (Grant No. EP/J018678/1 and EP/M01326X/1). The authors also wish to thank all the technical staff of James Watt Nanofabrication Centre (JWNC) at the University of Glasgow for their assistance.

References

[1] Y.T. Gau, L.K. Dai, S.P. Yang, P.K. Weng, K.S. Huang, Y.N. Liu, C.D. Chiang, F.W. Jih, Y.T. Cherng, H. Chang, 256 × 256 InSb focal plane arrays, Proc. SPIE 4078, Optoelectronic Materials and Devices II, 467, July 11, 2000http://dx.doi.org/10.1117/12.392175.

[2] K.-M. Chang, J.-J. Luo, C.-D. Chiang, K.-C. Liu, Wet etching characterization of InSb for thermal imaging applications, Jpn. J. Appl. Phys. 45 (2006) 1477–1482, http://dx.doi.org/10.1143/JJAP.45.1477.

[3] J. Moore, H. Hendriks, A. Morales, Characterization and control of galvanic corrosion during GaAs wafer photoresist processing, Proc. 2003 International Conference on Compound Semiconductor Manufacturing Technology (GaAs Mantech), 2003 (Paper No 8.8.).

[4] S.J. Pearton, U.K. Chakrabarti, W.S. Hobson, A.P. Perley, Cl_2 and $SiCl_4$ reactive ion etching of In-based III–V semiconductors, J. Electrochem. Soc. 137 (10) (1990) 3188–3202, http://dx.doi.org/10.1149/1.2086185.

[5] G. Zhang, W. Sun, S. Xu, H. Zhao, H. Su, H. Wang, Inductively coupled plasma reactive ion etching of InSb using CH_4/H_2/Ar plasma, J. Vac. Sci. Technol. A 27 (2009) 681–685, http://dx.doi.org/10.1116/1.3143664.

[6] S.J. Pearton, U.K. Chakrabarti, E. Lane, A.P. Perley, C.R. Abernathy, W.S. Hobson, K.S. Jones, Characteristics of III–V dry etching in HBr-based discharges, J. Electrochem. Soc. 139 (3) (1992) 856–864, http://dx.doi.org/10.1149/1.2069316.

[7] G.A. Vawter, J.R. Wendt, Chlorine reactive ion beam etching of InSb and $InAs_{0.15}Sb_{0.85}$/InSb strained-layer superlattices, Appl. Phys. Lett. 58 (1991) 289–291, http://dx.doi.org/10.1063/1.104664.

[8] J. Sun, J. Kosel, Room temperature inductively coupled plasma etching of InAs/InSb in BCl_3/Cl_2/Ar, Microelectron. Eng. 98 (2012) 222–225, http://dx.doi.org/10.1016/j.mee.2012.07.018.

[9] M. Levinshtein, S. Rumyantsev, M. Shur, Handbook Series on Semiconductor Parameters, vol. 1World Scientific, Singapore, 1996.

[10] H.D. Trinh, Y.C. Lin, E.Y. Chang, C.-T. Lee, S.-Y. Wang, H.Q. Nguyen, Y.S. Chiu, Q.H. Luc, H.-C. Chang, C.-H. Lin, S. Jang, C.H. Diaz, Electrical characteristics of Al_2O_3/InSb MOSCAPs and the effect of post-deposition annealing temperatures, IEEE Trans. Electron Devices 60 (5) (May 2013) 1555–1560, http://dx.doi.org/10.1109/TED.2013.2254119.

[11] C. Seok, M. Choi, S. Park, J. Jung, Y. Park, I.-S. Yang, E. Yoon, Raman spectroscopy of the damages induced by Ar-ion beam etching of InSb(100) surface, ECS Solid State Lett. 3 (3) (Dec. 2014) 27–29, http://dx.doi.org/10.1149/2.009402ssl.

[12] C. Xie, V. Pusino, A. Khalid, M. J. Steer, M. Sorel, I. G. Thayne and D. R. S. Cumming, Monolithic integration of an active InSb-based mid-infrared photo-pixel with a GaAs MESFET, accepted for publication on IEEE Electron Devices, Transactions on.

[13] J.R. Mileham, J.W. Lee, E.S. Lambers, S.J. Pearton, Dry etching of GaSb and InSb in CH_4/H_2/Ar, Semicond. Sci. Technol. 12 (3) (1997) 338–344 (DOI: 0268-1242/12/3/016).

[14] J. Abautret, A. Ervigen, J.P. Perez, Y. Laaroussi, A. Cordat, F. Boulard, P. Christol, Gas mixture influence on the reactive ion etching of InSb in an inductively coupled methane-hydrogen plasma, Semicond. Sci. Technol. 30 (6) (May 2015) 065014, http://dx.doi.org/10.1088/0268-1242/30/6/065014.

[15] G.A. Porkolab, P. Apiratikul, B. Wang, S.H. Guo, C.J.K. Richardson, Low propagation loss AlGaAs waveguides fabricated with plasma-assisted photoresist reflow, Opt. Express 22 (7) (Mar. 2014) 7733–7743, http://dx.doi.org/10.1364/OE.22.007733.

[16] C. Seok, M. Choi, I.-S. Yang, S. Park, Y. Park, E. Yoon, Multi-step plasma etching process for development of highly photosensitive InSb mid-IR FPAs, Infrared Technology and Applications XL, Proc. Of SPIE, vol. 9070 2014, p. 907018, http://dx.doi.org/10.1117/12.2053215.

[17] J.R. Sendra, J. Anguita, J.J. Pérez-Camacho, F. Briones, Reactive ion beam etching of aluminium indium antimonide, gallium indium antimonide heterostructures in electron cyclotron resonance methane hydrogen nitrogen silicon tetrachloride discharges at room temperature, Appl. Phys. Lett. 67 (22) (Nov. 1995).

[18] S.J. Pearton, C.R. Abernathy, F. Ren, Topics in Growth and Device Processing of III–V SemiconductorsChapter 8 World Scientific Publishing, 1996 456.

[19] J.-M. Lee, B.-I. Kim, S.-J. Park, Doping level-dependent dry-etch damage in n-type GaN, J. Electroceram. 17 (2) (Dec. 2006) 227–230, http://dx.doi.org/10.1007/S10832-006-6990-0.

[20] O.P. Agnihotri, H.C. Lee, K. Yang, Plasma induced type conversion in mercury cadmium telluride, Semicond. Sci. Technol. 17 (10) (Sept. 2002) R11, http://dx.doi.org/10.1088/0268-1242/17/10/201.

[21] M. de jesus Maciel, R.P. Rocha, J.P. Carmo, J.H. Correia, Measurement and statistical analysis toward reproducibility validation of AZ4562 cylindrical microlenses obtained by reflow, Measurement 49 (Mar. 2014) 60–67, http://dx.doi.org/10.1016/j.measurement.2013.11.056.

[22] I.G. Foulds, R.W. Johnstone, S.H. Tsang, M. Hamidi, M. Parameswaran, Polydimethylglutarimide (PMGI) as a structural material for surface micromachining, J. Micromech. Microeng. 18 (Mar. 2008) 045026 (DOI: 0960-1317/18/4/045026).